PHYS-E0411 Advanced Physics Laboratory

Synthesis and Measurement of Single-walled Carbon Nanotubes

A. Karakasidis, Q. Zhang, Y. Tian and E. I. Kauppinen

January 30. 2023

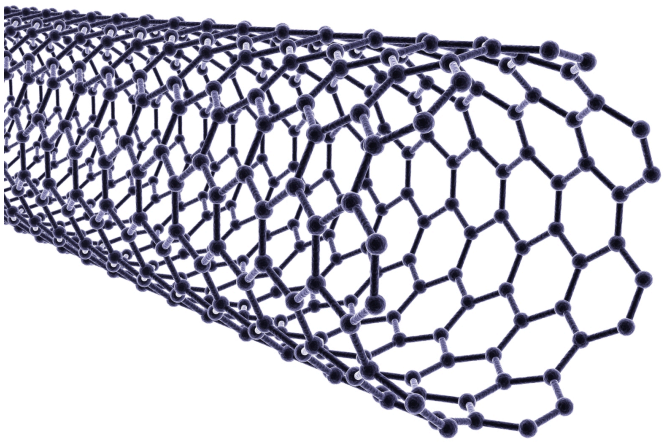

Table of Contents

1.Introduction

Carbon nanotubes are long hollow cylindrical nanostructures comprised solely of carbon atoms. Most of the fascination with this material, and many of its unique properties, stems from its unusual structure and aspect ratio. The cylinder is made up of a single layer of sp^2-bonded carbon, with a diameter of a few nanometers, and a typical length of several micrometers. Both single-walled and multiwalled forms of this material exist, but the physical properties of SWCNTs have proved to be much more interesting, and it is these that will be addressed in the following chapter. They can be considered as quasi one-dimensional (1D) systems and exhibit unusual electrical and mechanical properties.

1.1 Geometry of SWCNTs

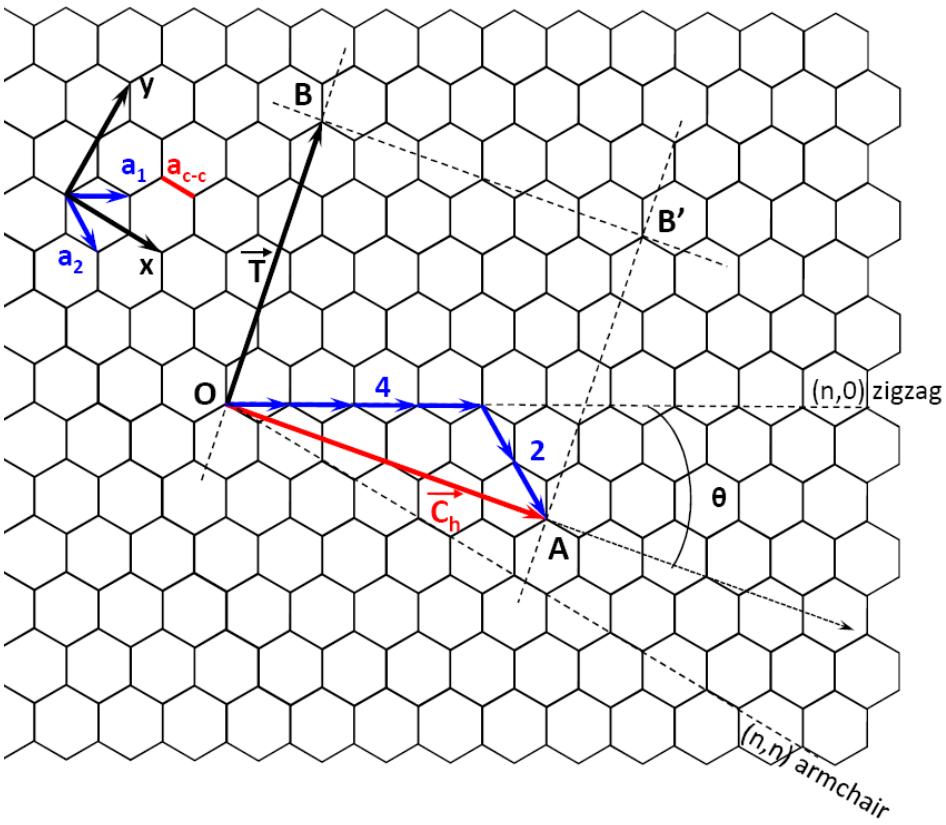

Figure 1.1 The unrolled honeycomb lattice of a nanotube. The $\overrightarrow{OA}$ and $\overrightarrow{OB}$ define the chiral vector C_h and the translation vector T of the nanotube, respectively. The figure corresponds to a chiral vector C_h = (4, 2) SWCNT. The chiral angle is indicated by θ.

A SWCNT is constructed by rolling a two-dimensional (2D) graphene sheet into a narrow cylinder (graphite is a layered 3D material, and a single layer of graphite is called 2D graphite, or a graphene layer). In Fig. 1.1, the unrolled honeycomb lattice of the nanotube is shown, in which $\overrightarrow{OB}$ is the direction of the nanotube axis, and the direction of $\overrightarrow{OA}$ corresponds to the equator [1]. By rolling the honeycomb sheet so that points O and A coincide, a carbon nanotube can be constructed. The chiral vector $\vec{C}_h$ fully determines the geometry of a SWCNT, and is expressed in terms of the real space unit vectors $\vec{a}_1$ and $\vec{a}_2$ of the hexagonal lattice:

$$\vec{C}_h = n\vec{a}_1 + m\vec{a}_2 \equiv (n,m)\,,\ (n,m \text{ are positive integers}, n \geq m) \qquad (1.1)$$

In Cartesian coordinates, the unit vectors $\vec{a}_1$ and $\vec{a}_1$ can be expressed as:

$$\vec{a}_1 = \left(\frac{\sqrt{3}}{2}a, \frac{a}{2}\right),\ \vec{a}_2 = \left(\frac{\sqrt{3}}{2}a, -\frac{a}{2}\right) \qquad (1.2)$$

where $|\vec{a}_1| = |\vec{a}_2| = a = \sqrt{3}a_{cc}$, and $a_{cc} = 1.42$ Å is the distance between neighboring carbon atoms. The diameter of the SWCNT is given by $d_t = |\vec{C}_h| = a\sqrt{n^2 + m^2 + nm}$. The angle θ that $\vec{C}_h$ makes with $\vec{a}_1$ is called the chiral angle, and from symmetry arguments $0 \leq \theta \leq 30^\circ$. The chiral angle θ can be defined by an expression involving cos(θ):

$$\cos\theta = \frac{\vec{C}_h \bullet \vec{a}_1}{|\vec{C}_h||\vec{a}_1|} = \frac{2n+m}{2\sqrt{n^2+m^2+nm}} \qquad (1.3)$$

Thus θ is related to the integers (n, m), defined in Eq.(1.1). If m=0, then $\theta = \cos^{-1}(1) = 0$, and the nanotubes are called 'zigzag' (n, 0) nanotubes, and if n=m, then $\theta = \cos^{-1}(\sqrt{3}/2) = 30°$, in this case the nanotubes are of the 'armchair' (n, n) variety. Otherwise, they are referred to as chiral (n, m) nanotubes.

The translation vector $\vec{T}$ is parallel to the nanotube axis and is normal to the chiral vector $\vec{C}_h$ in the unrolled lattice, as shown in Fig. 1.1. The lattice vector is defined as $\vec{T} = t_1\vec{a}_1 + t_2\vec{a}_2 \equiv (t_1, t_2)$, where:

$$t_1 = \frac{2m+n}{d_R}, t_2 = \frac{2n+m}{d_R} \tag{1.4}$$

The value d_R in equation (1.4) is the greatest common divisor (gcd) of (2m+n) and (2n+m). By introducing d as the greatest common divisor of n and m, d_R can be related to d by:

$$d_R = \begin{cases} d & if\ n-m\ is\ not\ a\ multiple\ of\ 3d \\ 3d & if\ n-m\ is\ a\ multiple\ of\ 3d \end{cases} \tag{1.5}$$

The vectors $\vec{C}_h$ and $\vec{T}$ define the rectangle OAB'B in Fig. 1.1, which encloses the unit cell of the SWCNT. The number of hexagons in the unit cell is N, where:

$$N = \frac{\left|\vec{C}_h \times \vec{T}\right|}{\left|\vec{a}_1 \times \vec{a}_2\right|} = \frac{2(m^2 + n^2 + nm)}{d_R} \tag{1.6}$$

It should be noted that each hexagon contains two carbon atoms. Thus there are 2N carbon atoms in each unit cell of such carbon nanotubes.

One then can image there are many possible (n,m) combinations, give rise to many possible SWCNT structures. A chiral mapping of (n,m) SWCNTs are given in the Figure 1.2. These SWCNT structures fall into three general categories (zigzag, chiral and armchair), examples of which are shown in Fig 1.3 along with a transmission electron microscope image of SWCNTs.

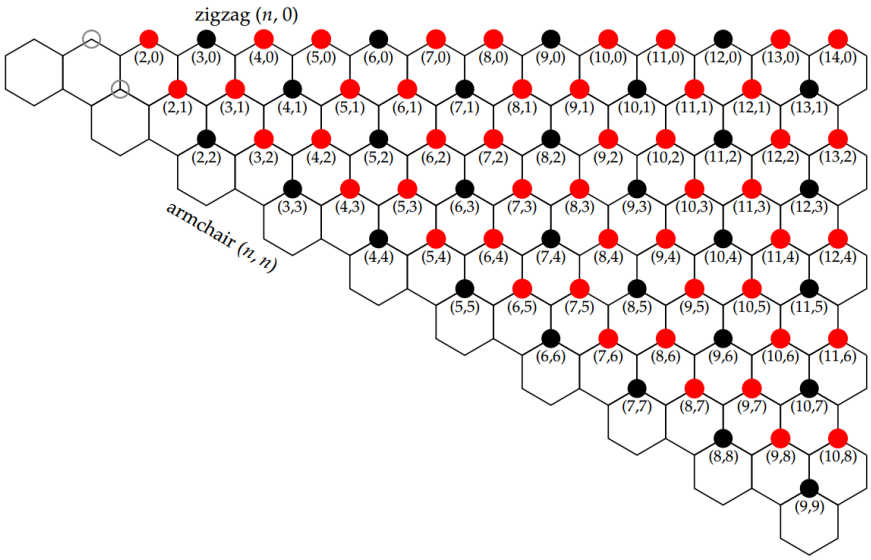

Figure 1.2 The chiral map of (n,m) SWCNTs, where each dot corresponds to a specific chirality. The SWCNT structure is specified either by two integers (n,m) or equivalently, a combination of diameter d and chiral angle θ. The red dots represent semiconducting nanotubes, while the black dots are for metallic nanotubes. Adapted with permission from [3].

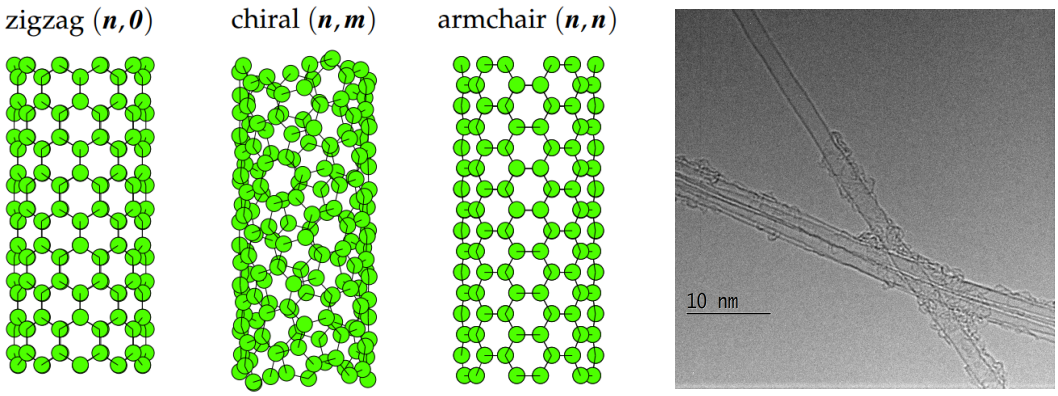

Figure 1.3 Three SWCNT geometries, zigzag, chiral, and armchair. Adapted with permission from [3]. The far-right image shows the high-resolution transmission electron microscope (HRTEM) image of SWCNTs.

1.2 Electronic Structure of SWCNTs

The electronic structure of SWCNTs is derived via a simple tight-binding (TB) calculation for the π-electrons of carbon atoms, which are the most important electrons for determining the solid-state properties of the material. Since many physical properties of SWCNTs are very similar to those of other carbon systems, particularly graphite/graphene [2], it is often convenient to begin with the well-known properties of

graphite, and then consider them in the 1D geometry of a SWCNT. The energy dispersion relations for 2D graphite are shown in Fig. 1.4.

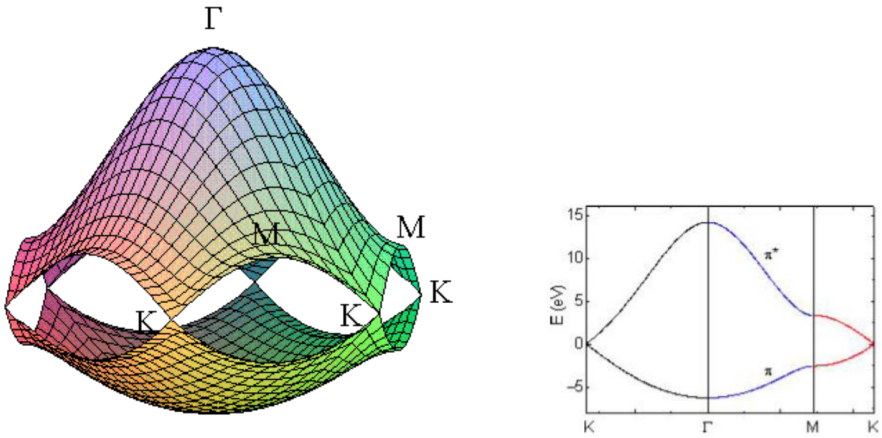

Figure 1.4 The energy dispersion relations for 2D graphite are shown throughout the whole region of the Brillouin zone. The labels indicate the high symmetry points. The right figure shows the energy dispersion along the high symmetry directions of the triangle ΓMK shown in Fig. 1.4. Adapted with permission from [3].

We can now consider the periodic boundary conditions that result from wrapping the graphene sheet into a tubular structure. The electron wave vector associated with the translation vector $\vec{T}$ (along the nanotube axis) remains continuous for a nanotube of infinite length, while the wave vector along the nanotube circumferential direction, denoted by chirality vector $\vec{C}_h$, becomes quantized. The remaining allowed wave vectors can be represented as a set of lines in the dispersion relation of graphene (Fig. 1.4). When the energy dispersion relation of graphene is denoted by E_{g2D}, the N pairs of the 1D energy dispersion relations of a SWCNT are given by:

$$E_\mu(k) = E_{g2D}(k\frac{K_2}{|K_2|} + \mu K_1), \quad \left(\mu = 1,\ldots,N, \; and \; -\frac{\pi}{T} < k < \frac{\pi}{T}\right) \tag{1.7}$$

Here, k denotes the wave number along the SWCNT axis, and the cuts are made on the lines of $kK_2/|K_2| + \mu K_1$. The energy dispersion curves described by Eq. 1.7 correspond to the cross sections of the 2D energy dispersion surface shown in Fig. 1.3.

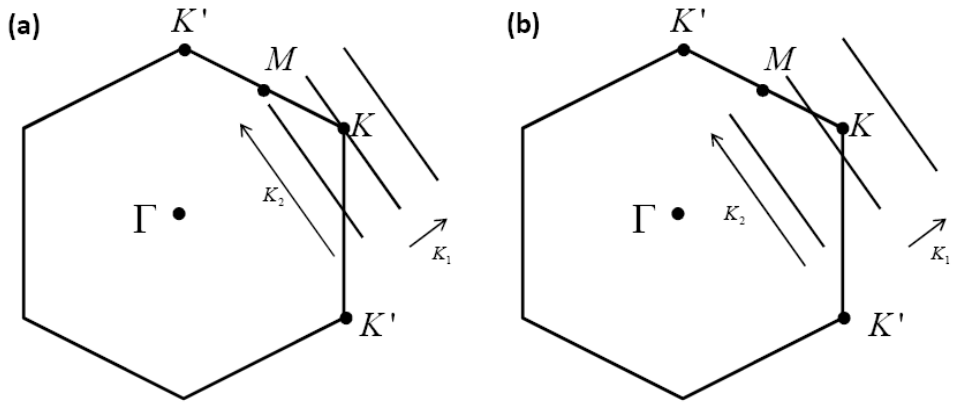

Figure 1.5 The wave vector k for 1D SWCNTs is represented in the 2D Brillouin zone of graphite (hexagon) as bold lines for (a) metallic and (b) semiconducting SWCNT. (a) For metallic nanotubes, the bold line (allowed state) intersects a K point at the Fermi energy of graphite. (b) For semiconducting nanotubes, the bold line does not go through a K point, with a finite energy band gap. Adapted with permission from [3].

If for a particular (n, m) nanotube, the cutting line passes through a K point of the 2D Brillouin zone (Fig. 1.5 (a)), where the π and π * energy bands of 2D graphite are degenerate due to symmetry, and the 1D energy bands have a zero-energy gap, and therefore they are metallic (M) carbon nanotubes. If, however, the cutting line does not pass through a K point, then the SWCNT exhibits semiconducting (S) behaviour, with a finite energy gap between the valence and conduction bands (see Fig. 1.5 (b)). From these geometrical arguments it can be derived that SWCNTs with indices (n, m) where mod (n-m, 3) =0 are metallic, whereas SWCNTs for which mod (n-m, 3) $\neq$ 0 are semiconducting. As shown in the chiral (n,m) map in Figure 1.2, the black and red dots correspond to metallic and semiconducting SWCNTs, respectively.

Since the SWCNT is a 1D system, the electronic density of states (DOS) vs. energy presents the characteristic van Hove singularities (vHs). Fig.1.6. shows examples of the calculated density of states (DOS) for (4, 2) semiconducting and (5, 5) metallic SWCNTs.

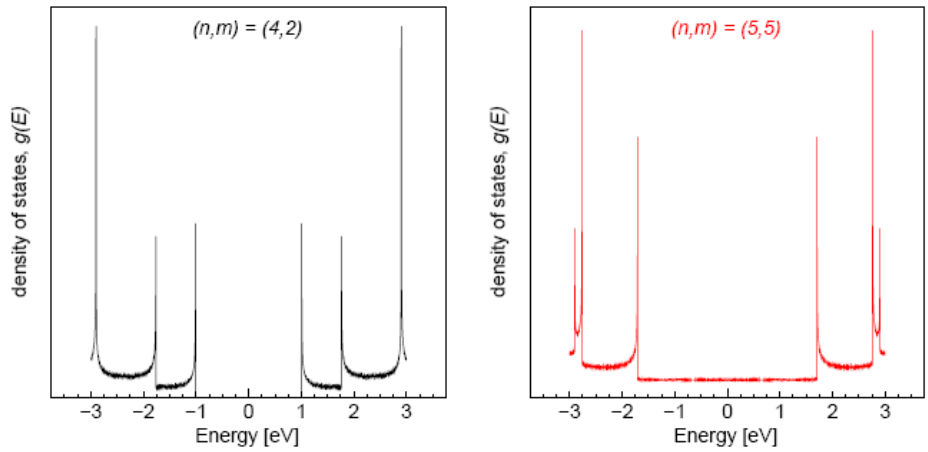

Figure 1.6. Plots of the density of states for a semiconducting (4, 2) chiral SWCNT, and a metallic (5, 5) armchair SWCNT. Images are from [4] with permission.

1.3 Optical Properties of SWCNTs

In general, the optical properties of carbon nanotubes refer specifically to absorption, photoluminescence, and Raman scattering. Since the electronic structure depends on the chirality of a given nanotube, experimental optical probes of the electronic structure can reveal much information about the diameter, chirality, and metallic or semiconducting nature of a SWCNT sample. In the following sections, two important optical spectroscopic techniques that are used to characterize SWCNTs are introduced.

1.3.1 Optical Absorption Spectroscopy

Optical absorption spectroscopy (OAS) measures the absorption of electromagnetic radiation. The absorption is a function of the frequency (or wavelength), due to the interaction of light with a sample. When light propagates through an absorbing medium, its intensity decreases exponentially according to the Beer-Lambert law,

$$I(L) = I_0 e^{-\alpha L c} \tag{1.8}$$

where I_0 is the intensity of the incident light, α is the absorption coefficient, L is the optical path length, and c is the concentration of an absorbing species in the material. This is illustrated in Fig. 1.7. By measuring the transmitted intensity relative to the incident intensity, the absorbance (for a given wavelength λ) is given by the following expression

$$A = -\ln\ (\frac{I}{I_0}) \tag{1.9}$$

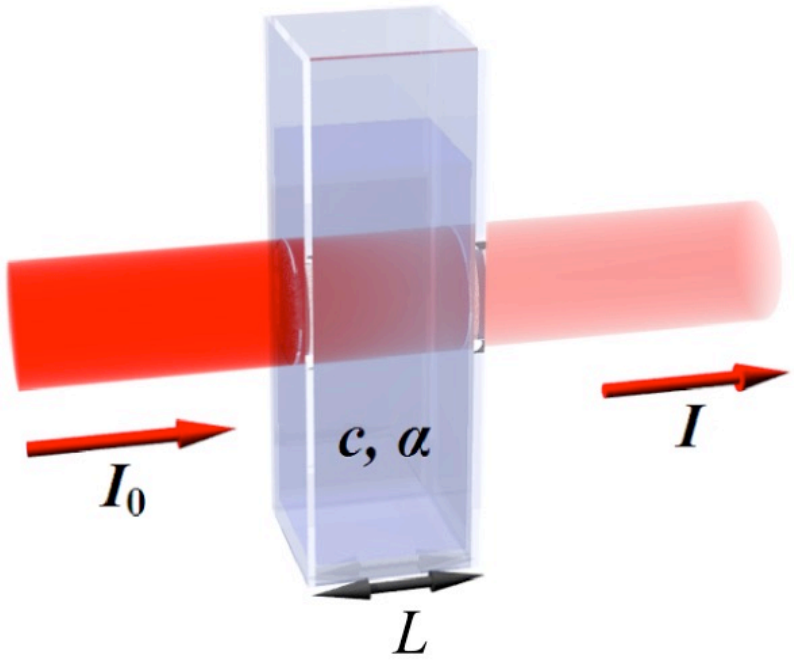

Figure 1.7 Illustration of Beer-Lambert absorption in a material with absorption coefficient ***α*** and concentration of absorbing species ***c***. The optical path length is ***L***, and ***I*** and ***I₀*** are the incident and transmitted intensities, respectively. (Image used with permission from Wikipedia)

In OAS, the wavelength of the incident light is scanned and usually covers the ultraviolet, visible, and near infrared (UV-Vis-NIR) regions of the spectrum. The optical response of SWCNTs is dominated by transitions between valence and conduction bands, where momentum conservation only allows transition pairs of singularities that are symmetrically placed with respect to the Fermi level. These vertical transitions are labeled $E_{ii}\ (i = 1,2,3,\ldots)$. Basically, light will be absorbed when in resonance with the E_{ii} values for the (n, m) nanotubes in a sample. Despite the fact that a SWCNT has a sharply peaked density of states, the peaks that are found in OAS are broad. The dominant reason for this is due to sample heterogeneity. An ensemble of nanotubes most often consists of many different species (n, m), each with a different set of absorption peaks, which add up to produce a broad peak that contains information about the diameter distribution in the sample. Thus OAS of SWCNTs is often used to evaluate the mean diameter (d_t) and diameter distribution of nanotubes in a sample, rather than the chiralities.

A typical absorption spectrum of bulk SWCNTs consists of three broad absorption peaks labelled E_{11}^S, E_{22}^S, E_{11}^M, which correspond to the first and second transition of S-SWCNTs, and the first transition of M-SWCNTs, respectively (see Fig.1.8). The energy of optical transitions in a SWCNT is inversely proportional to the nanotube diameter. Based on the tight-binding model, for the first two optical transitions in S-SWCNTs, it follows that $E_{11}^S = 2a_0\gamma_0/d$, $E_{22}^S = 4a_0\gamma_0/d$, where γ_0 is tight binding nearest neighbor overlap integral, d is the diameter. For the M-SWCNTs, the energies of the optical transitions are proportional to $E_{11}^M = 6a_0\gamma_0/d$. Therefore, the mean diameter d of SWCNT bulk sample is generally estimated based on the position of the peak E_{22}^S and use formula (1.10),

$$d_t = \frac{4a_0\gamma_0}{E_{22}^s} \qquad (1.10)$$

where $a_0 = 0.142\ \text{nm}$, $\gamma_0 = 3.0\ \text{eV}$. Furthermore, the diameter distribution can be obtained from the width of this absorption peak.

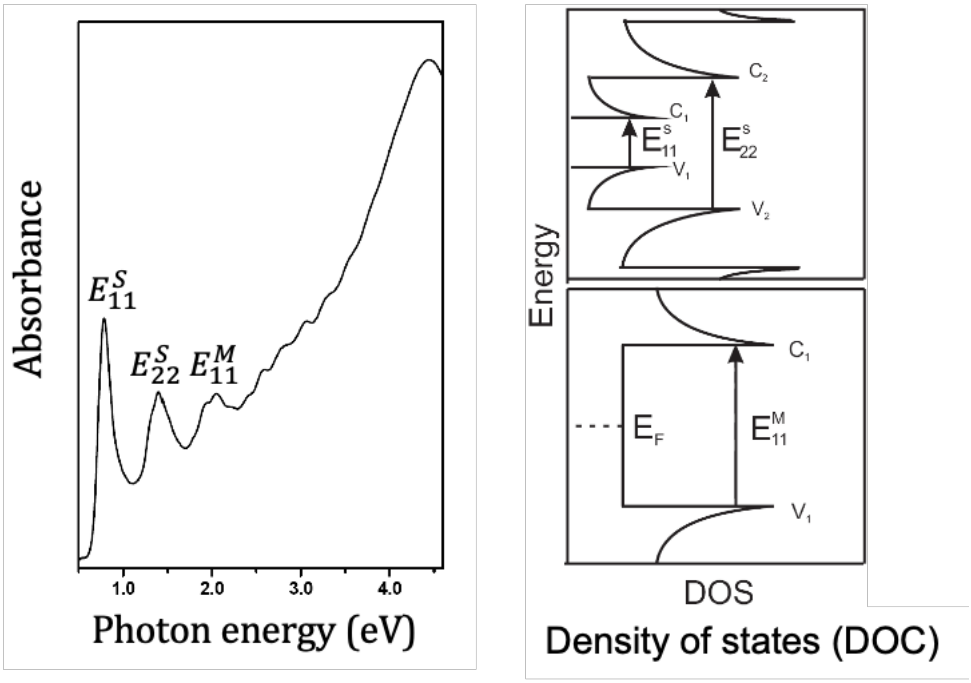

Figure 1.8 A typical optical absorption spectrum (left) of SWCNT solid sample showing three broad peaks that are associated with the first (E_{11}^S) and second (E_{22}^S) optical transitions for S-SWCNT and the first transition (E_{11}^M) for M-SWCNT. E_F is the Fermi level, while c and v are the conduction and valence bands, respectively.

1.3.2 Resonant Raman Spectroscopy

Raman scattering refers to the inelastic scattering of a photon off of a molecule. Most scattering events are elastic (Rayleigh) processes. However, a small fraction of incident photons can be inelastically scattered, by exchanging energy with the molecule as a result of interacting with optical phonons. There are two types of Raman scattering, known as Stokes scattering and anti-Stokes scattering. In both cases, the scattering process is described by three steps consisting of (i) an absorption of the incident photon ($\hbar\nu$) into an electronic excitation of the molecule, (ii) the generation or absorption of a phonon ($\hbar\omega$), and (iii) the emission of a photon ($\hbar\nu \mp \hbar\omega$) (see Fig.1.9).

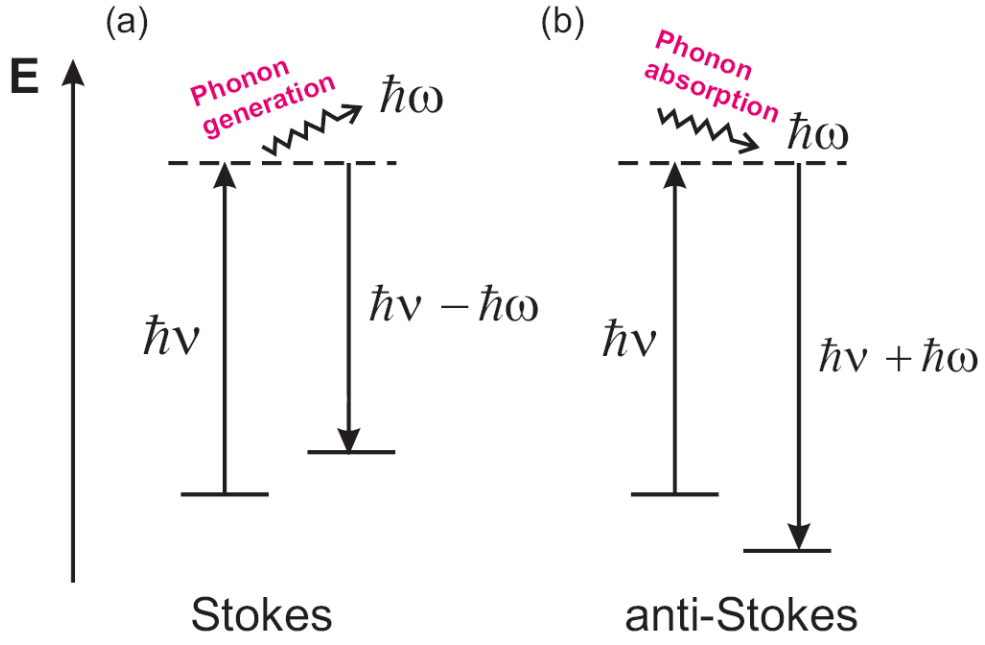

Figure 1.9 Energy level diagrams for (a) Stokes and (b) anti-Stokes Raman scattering processes. The incident photon energy is denoted by $\hbar\nu$, and by generating or absorbing a phonon with energy $\hbar\omega$, the (a) Stokes or (b) anti-Stokes scattered photon energy is $\hbar\nu \mp \hbar\omega$.

The probability for the Raman scattering process is very low (approximately 1 in 10^7 incident photons), because it involves an excitation to a virtual level that is only allowed for a very short time, in the context of the uncertainty principle. The probability is strongly increased, typically by a factor of 10^2-10^4, if the transition energy for either the absorbed or the emitted photon coincides with an electronic transition energy of the molecule. Observation of this process is called resonant Raman spectroscopy. In the case of SWCNTs, the cross section for a resonant Raman process is so large that it is even possible to analyze the

vibrational modes of an individual SWCNT. Furthermore, the Raman signals detected for different excitation energies can be used to identify SWCNTs with different chiralities at resonance. This makes Raman spectroscopy one of the most important optical techniques for characterizing SWCNTs.

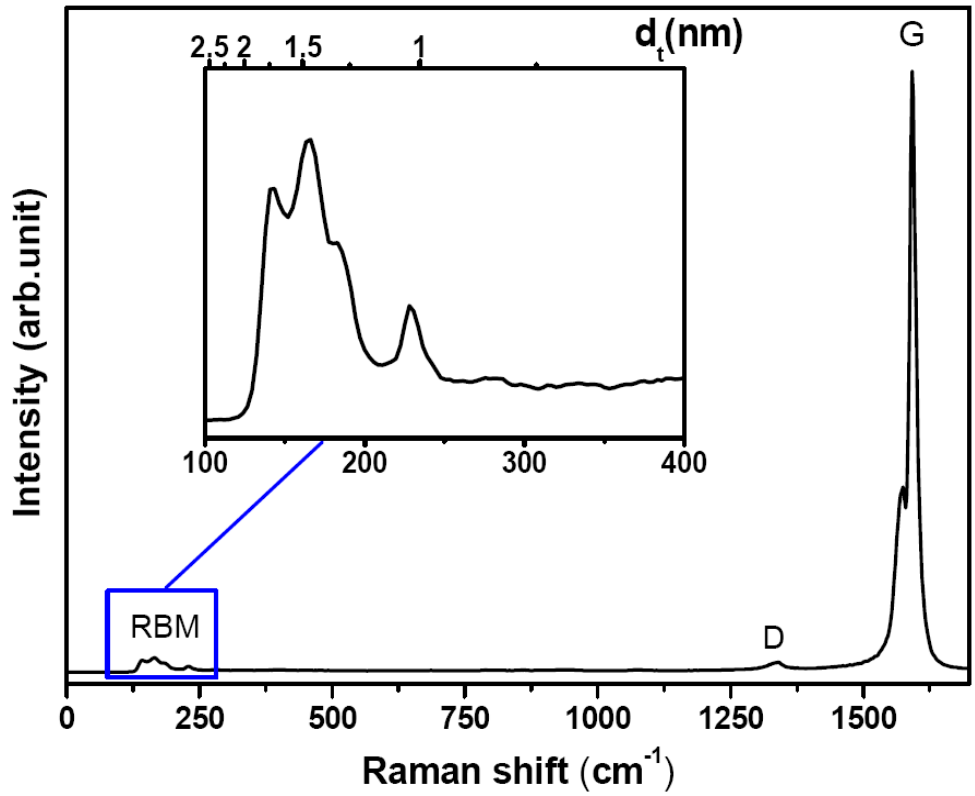

Figure 1.10 A typical Raman spectrum from a SWCNT thin film sample excited by a 533 nm laser. The inset shows the enlarged RBM peaks.

A typical Raman spectrum is shown in Fig. 1.10, where the Raman shift (i.e. the shift with respect to the excitation light wavenumber) is plotted in wavenumber units of cm^{-1}. The dominant peak located at ~1590 cm^{-1} in the figure is associated with the in-plane tangential optical phonon that involves the stretching of the bond between the two atoms in the graphene unit cell (as shown in Fig. 1.11 (a)) [2]. For this reason, this band is referred to as the graphite-like band, or simply the G band. While the G band in graphite exhibits a single Lorentzian peak at ~1582 cm^{-1}, the G band of SWCNTs splits into a lower energy G^- peak and a higher energy G^+ peak. This splitting is caused by the curvature of SWCNTs, which induces an energy difference between the axial and transverse in-plane vibrational modes. Interestingly, it has been shown that the G^- feature is strongly sensitive to whether the nanotube is metallic or semiconducting, exhibiting a Breit-Wigner-Fano (BWF) lineshape for

the case of metallic nanotubes. In addition, the frequency of G^+ peak is independent of both diameter and chiral angle, while the G^- feature shows a dependence on the nanotube diameter. The scattering process associated with G band excitation is a first-order process, meaning that only one scattering event occurs. Second-order scattering events can occur when excited phonons are scattered by defects or inconsistencies in the crystal lattice. This shows up in the Raman spectra of SWCNTs as a small peak near 1350 cm^{-1} , which is called the disorder band, or D-band. The ratio of the *G*/*D* modes in Raman spectra is conventionally used to quantify the structural quality of carbon nanotubes.

The last major Raman feature visible in the spectrum in Fig. 1.10 is the series of peaks below 400 cm^{-1}. These peaks are the result of a phonon excitation that is unique to SWCNTs, and they contain much information about the SWCNTs that make up the sample. The G-band mode described above is caused by a resonant in-plane vibrational mode, which is characteristic of graphite. An out-of-plane mode also exists, where the vibration is perpendicular to the lattice plane. If one imagines taking a graphene sheet supporting such an out-of-plane vibration, and rolling it into the cylindrical shape of a SWCNT, the out-of-plane vibrations become oriented radially away from the SWCNT axis, as shown in Fig. 1.11 (b). The result is a purely radial mode, where the diameter of the entire SWCNT oscillates, appearing as though it were “breathing”. For this reason, this mode is known as the radial breathing mode, or RBM [4]. The Raman intensity of the RBM is strongly enhanced when the incident photon is in resonance with the energy gap E_{ii} of a SWCNT. Theoretical and experimental studies show that the RBM frequency ω_{RBM} is inversely proportional to the nanotube diameter d_t, and can be expressed by the relationship:

$$\omega_{RBM} = \frac{A}{d_t} + B, \tag{1.11}$$

where A=217.8 and B=15.7 are values determined experimentally. Because of its dependence on the nanotube diameter, the spectrum of this mode is largely used to characterize of the diameter properties of SWCNTs.

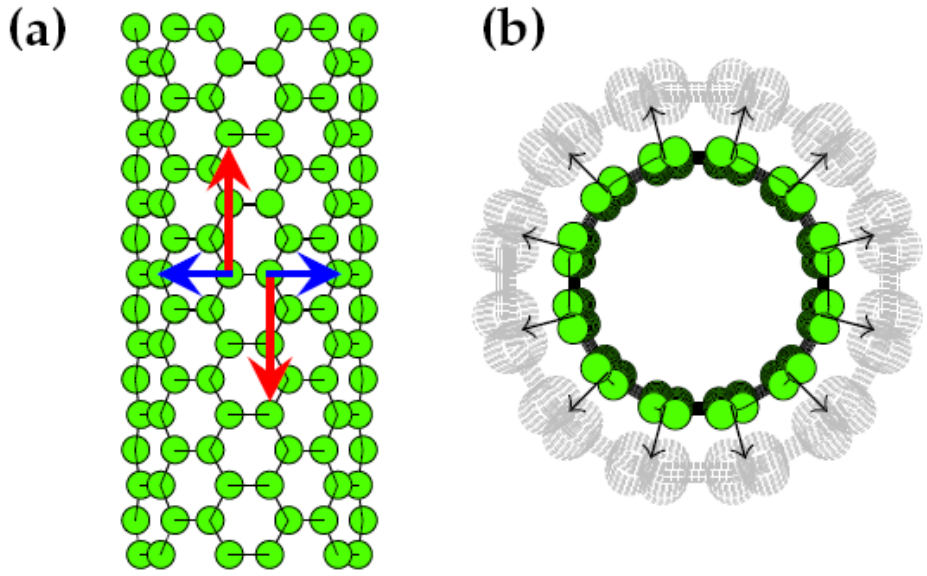

Figure 1.11 (a) the in-plane vibrational modes corresponding to the G band Raman signal, and (b) the out-of-plane vibration that gives rise to radial breathing mode excitations. Images are from [4], used with permission.

It is worth noting that, while a single Raman measurement provides information about the tubes that are in resonance with a particular laser line, it does not give a complete characterization of the distribution of diameters in the SWCNT sample. However, by collecting Raman spectra produced by many different laser lines, a good characterization of the diameter distribution can be obtained. Furthermore, when referring to the Kataura plot [5-6] (Fig. 1.12 (b)), it is feasible to assign the RBMs to specific chiralities (or at least to particular 2n+m families) of SWCNTs. Determine the position of the peaks in RBM in the Raman spectrum like on Fig. 1.12 (a) will be quite simple to determine the chirality of nanotubes corresponding to them. For that use the Kataura plot in Figure 1.12 (b), a horizontal line that corresponds to the energy of the laser with which the measurement was made, we can see that the line crosses several points on the chart, some of which coincide with the peaks. Each point corresponds to certain chirality. If the points are located close to each other, you can find family and it helps to classify the type of nanotubes.

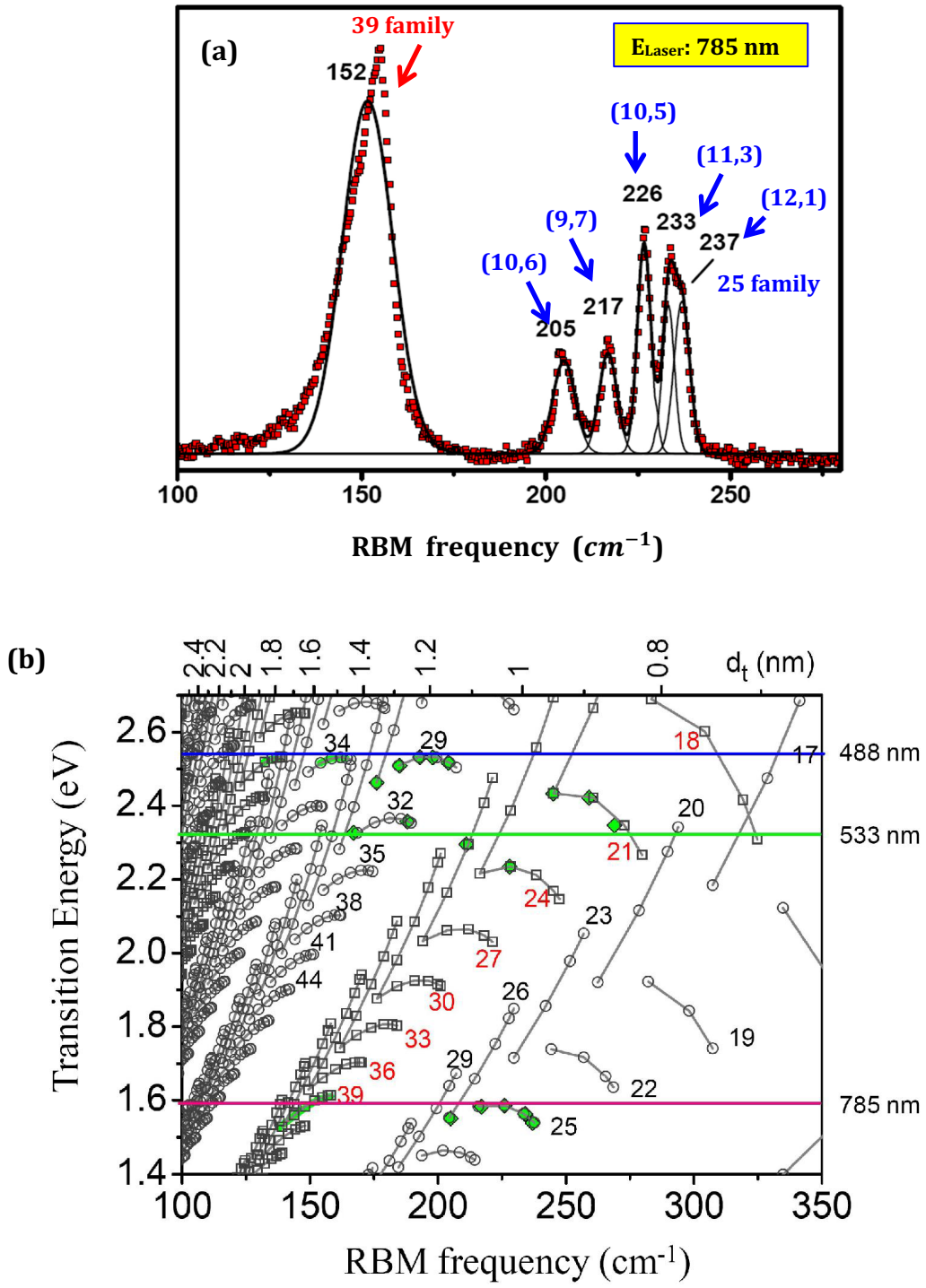

Figure 1.12 (a) RBM Raman spectrum of a SWCNT sample excited by 785 nm laser. The chirality (n,m) or/and families are also indicated in the spectrum based on the Kataura plot shown in (b). The values of optical transition energy E_{ii} as calculated with ETB/MB model for semiconducting (circles) and metallic (squares) tubes vs. radial breathing mode frequency (bottom horizontal axis) and nanotube diameter (top horizontal axis). The 2n+m = constant families are joined by solid lines, and the family numbers are also indicated.

1.3.3 Sheet resistance

Sheet resistance (also known as surface resistance or surface resistivity) is a common electrical property used to characterise thin films of conducting and semiconducting materials. It is a measure of the lateral resistance through a thin square of material, i.e. the resistance between opposite sides of a square. The key advantage of sheet resistance over other resistance measurements is that it is independent of the size of the square - enabling an easy comparison between different samples. This property can easily be measured using a four-point probe and is critical in the creation of high-efficiency perovskite photovoltaic devices, where low sheet resistance materials are needed to extract charge [9-13].

1.3.3.1 The Four-Probe Method

The primary technique for measuring sheet resistance is the four-probe method (also known as the Kelvin technique), which is performed using a four-point probe. A four-point probe consists of four equally spaced, co-linear electrical probes, as shown in the schematic below:

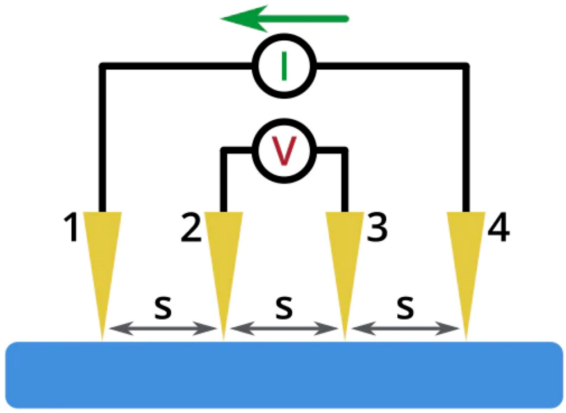

Figure 1.13 Schematic illustration of 4-probe measurement [9]

The sheet resistance can then be calculated using the following equation:

$$R_s = \frac{\pi}{\ln(2)} \frac{\Delta V}{I} = 4.53236 \frac{\Delta V}{I} \qquad (1.12)$$

R_s is the sheet resistance, ΔV is the change in voltage measured between the inner probes, and I is the current applied between the outer probes. The sheet resistance is generally measured using the units Ω/sq (ohms per square), to differentiate it from bulk resistance [7-11].

It should be noted that this equation is only valid if:

- The material being tested is no thicker than 40% of the spacing between the probes
- The lateral size of the sample is sufficiently large

If this is not the case, then geometric correction factors are needed to account for the size, shape, and thickness of the sample. If the thickness of the measured material is known, then the sheet resistance can be used to calculate its resistivity:

$$\rho = R_s t \qquad (1.13)$$

where ρ is the resistivity, and t is the thickness of the material.

2. Synthesis reactor and measurement equipment

2.1 Synthesis reactor

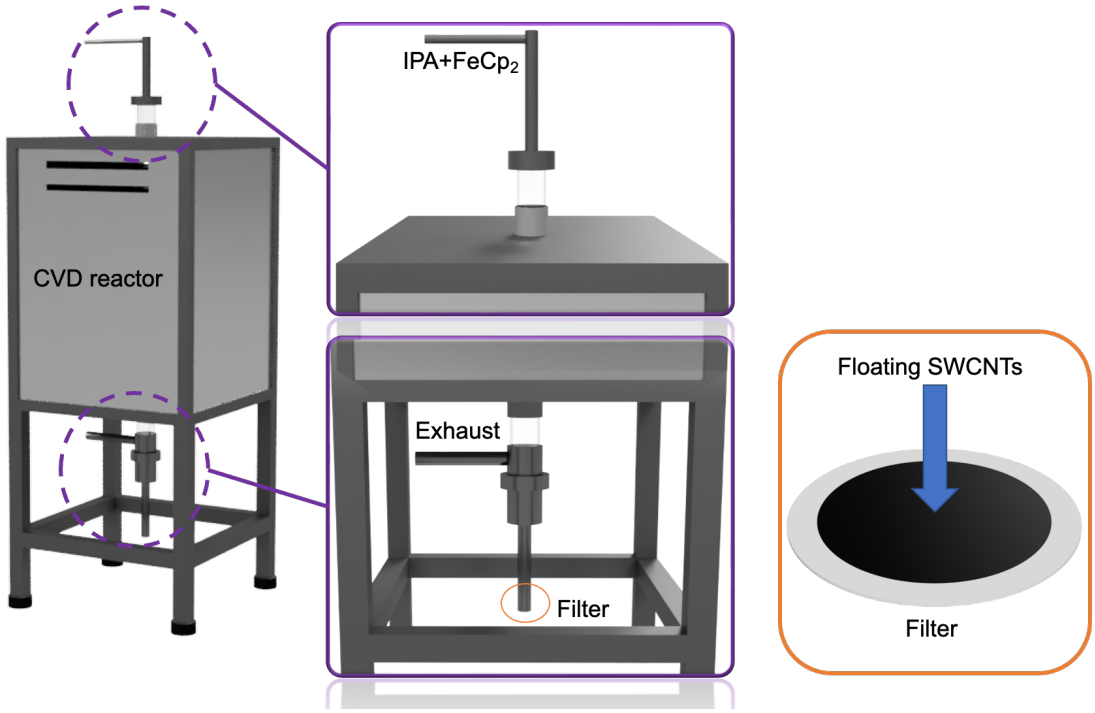

Figure 2.1 3D Schematic illustration the synthesis reactor. IPA solution was introduced to the reactor using a syringe pump system. The SWCNTs are collected at the reactor outlet using a membrane filter [12].

The SWNTs were synthesized using a liquid feed floating catalyst chemical vapor decomposition (FC-CVD) method with iron (Fe) particles as catalysts and isopropyl alcohol (IPA) as carbon precursor (Fig. 2.1). IPA solution containing 0.25 wt% ferrocene, and a small amount of thiophene (molar ratio of sulfur to iron is in the range of 0.125-0.175) was sonicated for 1 min in a vial to form a homogeneous solution which was injected into a heating line using a syringe

pump at a feeding rate of 1-4 μl/min. The evaporated precursors in the heating line at 130 ºC were carried by 300 standard cubic centimeters (sccm) N2 and 30-60 sccm H_2. The reactor temperature for SWCNT synthesis was adjusted at 880 ºC [12]. As-produced SWCNTs were collected at the reactor outlet using a patterned ϕ25 mm membrane filter.

2.2 UV-Vis-NIR spectrometer

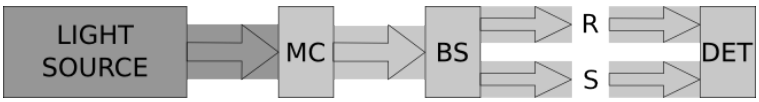

Figure 2.2 A simplified schema of the UV-Vis-NIR spectrometer. Light source is a tungsten or deuterium lamp, MC is the monochromator, BS is the beam splitter, R and S refer to the reference and sample, respectively, and DET is the detector [8].

The instrument used for measuring the PBG samples is a UV-Vis-NIR spectrophotometer (Perkin-Elmer Lambda 950 UV-Vis-NIR spectrophotometer). The instruction please see the 2.1 Section in exercise material of Photonic Bandgap Materials [13].

2.3 Raman spectrometer

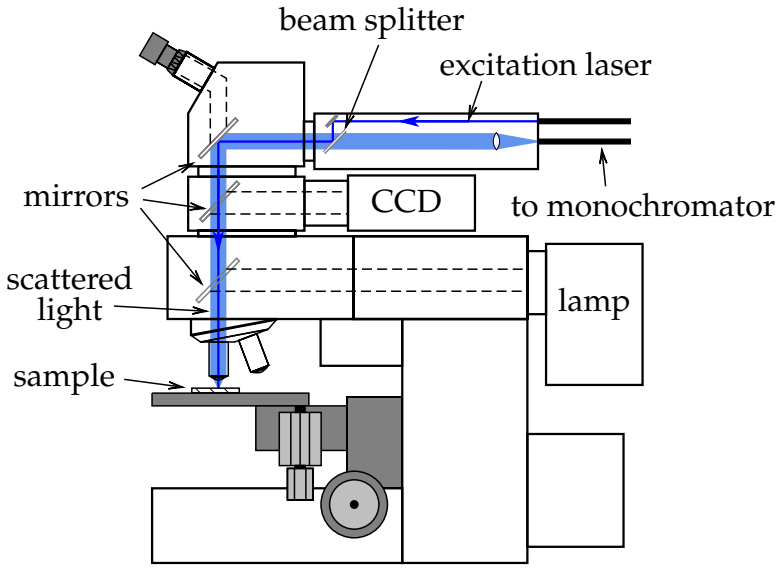

Figure 2.3 A diagram of the Raman spectrometer. The excitation sources are 488, 514 and 633 nm lasers. The scattered light is focused into an optical fiber, which sends it to a monochromator where the signal is recorded by a CCD [4].

As previously mentioned, there is a small probability that an incident photon will be inelastically scattered by a material. This occurs in roughly one of every 10^7 scattering events (the rest of which are scattered by the Rayleigh process). As a result, the intensity of Raman-scattered light is very weak, so in order to obtain a decent measurement of this signal it is necessary to increase the frequency of scattering events. One way to accomplish this is to use a laser as the light source, unlike in optical absorption spectroscopy, where a lamp is sufficient. To further enhance the Raman scattered signal, the laser is focused to a small area on the sample from where the signal is measured. This is often done by passing the laser through the lenses of an optical microscope, as illustrated in Fig. 2.3. Fortunately, the microscope lens can also be used to collect the scattered light, which is sent into a monochromator and recorded by a CCD. Before entering the monochromator, the intense Rayleigh signal is filtered out by a combination of a dichroic mirror (beam splitter) and an adjustable edge filter. A typical Raman spectrum is shown in Fig. 1.10, where the Raman shift – the shift with respect to the excitation light – is plotted in inverse cm.

2.4 Sheet resistance

The measurements of the SWCNTS thin film sheet resistance are going to be performed via a Jandel RM3000+ Test Unit (Figure 2.4). By applying a DC current (**I**) between the outer two probes and measuring the resultant voltage drop between the inner two probes, the sheet resistance can be calculated using the previously discussed Equation 1.12.

Figure 2.4 Jandel RM3000+ Test Unit

3. Exercise instructions

3.1 Synthesize SWCNT thin films

- When working in the lab, always use protective glasses and gloves. They are available in the lab.
- Firstly, learn the principles of the synthesis CVD reactor. Introduction to the 'real' reactor by the assistant.
- Operate the synthesis reactor at growth conditions of SWCNTs, i.e., N_2 at 300 sccm, H_2 flow at 30-60 sccm, feeding rates of 1-4 µl/min and the reactor temperature at 880 ^oC.
- Collect SWCNT thin film sample on the filter paper.
- Transfer the SWCNT thin films from filter paper onto quartz slide for the optical and thin film resistance measurements.

3.2 Measure the absorption spectra of your SWCNT thin film on quartz substrate

- Before the absorption measurements, do calibration of 0% and 100% transmittance without any samples in the compartment of spectrometer.
- Put clean quartz slide on the reference beam pass, and another quartz slide with SWCNT thin film on the sample beam pass, then measure the UV-Vis-NIR absorption spectra of SWCNTs.
- Compare the absorption features with the electronic structure of SWCNTs and get diameter properties of your sample.

3.3 Measure the Raman spectra of your SWCNT thin film on quartz substrate

- You'll receive instructions on how to use the Raman spectrometer.
- Focus the SWCNT sample surface by using optical lens in the Raman spectrometer.
- Move to the Raman mode, measure and acquire the Raman spectra of SWCNTs with laser source of 514 nm.

3.4 Measure the sheet resistance of your thin film SWCNT samples on quartz substrate

- Measure the sheet resistance (R_s) of the thin films.

References

[1] R. Saito, G. Dresselhaus, M. S. Dresselhaus, Physical Properties of Carbon Nanotubes, Vol. 3, Imperial College Press, London 1998; Y.Tian, in Departmen of Applied Physics, Doctor of Philosophy, Aalto University School of Science, Helsinki 2012.
[2] A.Jorio, G. Dresselhaus, M. S. Dresselhaus, Carbon nanotubes: Advanced Topics in the Synthesis, Structure, Properties and Applications, Springer, Heidelberg 2008.
[3] H. M. Cheng, F. Li, G. Su, H. Pan, M. Dresselhaus, Applied Physics Letters 1998, 72, 3282.
[4] Erik.Einarsson, in Department of Mechanical Engineering, Doctor of Philosophy, The University of Tokyo, Tokyo 2006.
[5] M. S. Dresselhaus, G. Dresselhaus, R. Saito, A. Jorio, Annual Review of Physical Chemistry 2007, 58, 719.
[6] H. Kataura, Y. Kumazawa, Y. Maniwa, I. Umezu, S. Suzuki, Y. Ohtsuka, Y. Achiba, Synthetic Metals 1999, 103, 2555.
[7] https://www.ossila.com/en-eu/pages/sheet-resistance-theory#sheet-resistance-derivation.
[8] I. Miccoli, F. Edler, H. Pfnür, C. Tegenkamp, The 100th anniversary of the four-point probe technique: the role of probe geometries in isotropic and anisotropic systems, J. Phys.: Condens. Matter 2015, 27, 223201.
[9] L. B. Valdes, Resistivity Measurements on Germanium for Transistors, Proceedings of the I.R.E 1954, 420.
[10] H. Topsøe, Geometric Factors in Four Point Resistivity Measurement, 1966.
[11] F. M. Smits, Measurement of Sheet Resistivities with the Four-Point Probe, Bell Syst. Tech. J. 1958, 711.
[12] Er-Xiong Ding, Peng Liu, Abu Taher Khan, Qiang Zhang, Nan Wei, Hua Jiang, Esko I. Kauppinen, Towards the synthesis of semiconducting single-walled carbon nanotubes by floating-catalyst chemical vapor deposition: Challenges of reproducibility, Carbon 2022, 195, 92-100.
[13] J. Korhonenj, J. Vapaavuori and J. Hassinen., PHYS-E0411 Advanced Physics Laboratory Photonic Bandgap Materials, 23 Feb.2015.